Journal of Hazardous Materials Advances 7 (2022) 100133

Contents lists available at ScienceDirect

Journal of Hazardous Materials Advances

journal homepage: www.elsevier.com/locate/hazadv

Effect of the embedment of carbon doped nanocomposites in a real matrix on the enhanced photocatalytic activity

Arianna Menichetti[a], Moreno Guernelli[a], Gloria Guidetti[a], Andrea Cacciatore[b], Giampiero De Notarpietro[b], Marcello Molfetta[b], Claudia Capone[b], Matteo Calvaresi[a], Giuseppe Falini[a], Francesco Zerbetto[a], Iryna Polishchuk[c], Boaz Pokroy[c], Marco Goisis[b], Marco Montalti[a,*]

[a] Department of Chemistry "Giacomo Ciamician", University of Bologna, Via Selmi 2, Bologna 40126, Italy
[b] Italcementi S.p.A, I.Lab, Via Stezzano, 87, Bergamo 24126, Italy
[c] Department of Materials Science and Engineering, Technion – Israel Institute of Technology, Technion City, Haifa 3200003, Israel

ARTICLE INFO

Keywords:
Graphene
Titanium dioxide
Photocatalysis
Cement matrix
Air decontamination

ABSTRACT

Solar light can be used by semiconductor nanocrystals as a free and largely available source of energy to transform air pollutants into non-volatile less harmful chemicals. The efficiency of this process can be enhanced by doping the semiconductor with carbon-based materials, such as graphene. Nevertheless, such an increased activity has been reported (i) for nanocomposite photocatalysts produced on the research laboratory scale, (ii) analyzing their performance as self-standing photocatalysts and not after incorporation into "real" matrixes (e.g. building materials) and (iii) typically using model target pollutants instead of "real" hazardous ones. Here we describe the large-scale preparation of two series of carbon based photocatalysts starting from commercial materials and we demonstrate their superior photocatalytic activity in degrading important air pollutants as nitrogen oxides, compared to undoped photocatalysts. The photocatalytic activity was evaluated by NO_x abatement adopting the continuous flow procedure and the apparatus reported in the Italian standard UNI 11,247. Best performing materials were incorporated into two different inorganic matrixes (cement and lime). In both cases, the superior photocatalytic performances were maintained. An improvement up to 42±7% of the photocatalytic activity was measured in the case of a cement sample for a carbon-doped photocatalyst with respect to bare TiO_2. The materials were characterized by UV-Vis spectroscopy, high resolution powder X-ray diffraction (HR-PXRD), high-resolution scanning electron microscopy (HR-SEM) energy-dispersive X-ray spectroscopy (EDS) and micro-Raman.

1. Introduction

The design of photocatalytic materials for the effective use of solar light to eliminate organic pollutants (Tong et al., 2012) and photocatalysts integration into smart materials (Fleisch and Bahnemann, 2017) are hot topics for research as well as effective solutions for world-wide environmental challenges. Photocatalysts based on TiO_2, mainly in the form of anatase nanoparticles (TiO_2-NPs), are already on the market and embedded in commercial products, such as cement, because of their good compatibility with the inorganic cementitious matrix, low cost (3300 USD/Ton at 2021 prices, https://www.imcdgroup.com/en/imcd-stories/it-is-time-for-take-two-on-tio2) and stability in water (Hoffmann et al., 1995). The TiO_2-based photocatalysts application to cementitious materials, aimed to the degradation of environmental contaminants (Husken et al., 2009; Kovar et al., 2010; Ramirez et al., 2010; Zouzelka and Chemagazin, 2016) (e.g. NO, NO_2, SO_2, suspended organic particulate, volatile organic compounds, aromatic hydrocarbons, etc.), has mainly two goals: i) the self-cleaning effect of cementitious surfaces (Folli et al., 2009, 2012; Lai et al., 2016; Zailan et al., 2016) to preserve the original appearance of the surface of the building, often subjected to polluted environments; ii) the prevention from pollutants accumulation (Chen and Chu, 2011; Dalton et al., 2002; Dylla et al., 2011; Mamaghani et al., 2017; Poon and Cheung, 2007; Yu et al., 2016), according to the European Union (UN) environmental regulation directives (e.g. 2008/50/EC). However, TiO_2 can be activated as photocatalyst only with the UV part of the solar spectrum (Linsebigler et al., 1995) ($\Delta E \approx 3.25$ eV (Hoffmann et al., 1995)), that is just ~4% of the total solar radiation. For this reason, the efficacy of TiO_2-based photocatalysts incorporated in cement based materials is negligible in indoor conditions where the UV component of the solar light is not present (Tuchinda et al., 2006), and reduced in outdoor application. This means that ~96% of the useful energy to perform the photodegradation processes is wasted (Chen and Mao, 2007; Fujishima et al., 2008). Furthermore the 90% (Serpone et al., 1995) of sunlight that manages to activate TiO_2-NPs is lost because of the recombination of the photo-generated electron-hole pairs. Moreover, photocatalytic cement performances for

* Corresponding author.
E-mail address: marco.montalti2@unibo.it (M. Montalti).

https://doi.org/10.1016/j.hazadv.2022.100133
Received 21 April 2022; Received in revised form 18 July 2022; Accepted 22 July 2022

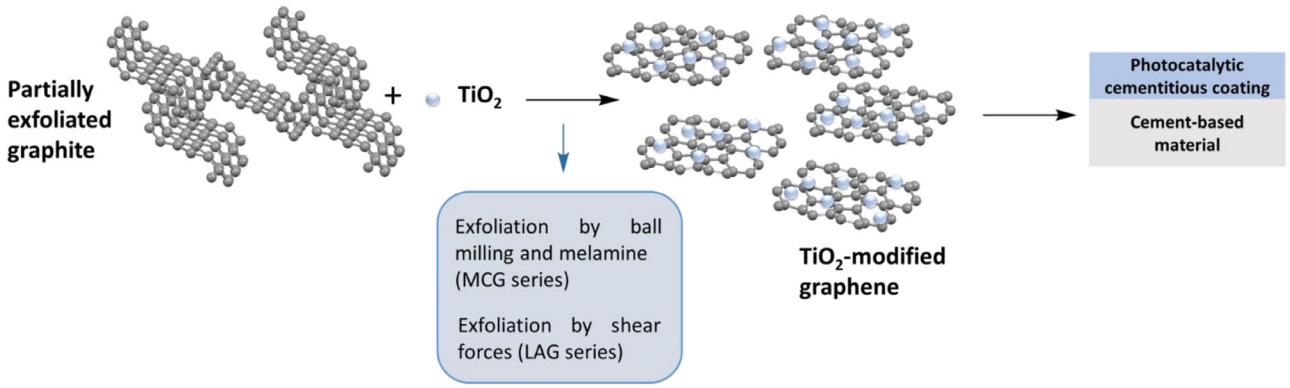

Scheme 1. Preparation of TiO_2-Graphene photocatalytic cementitious coatings by means of low-cost reactants and scalable methods.

outdoor applications are also limited because of effects which do not depend on the nature of the photocatalyst, such as sunlight intensity variations due to diurnal/seasonal changes and cloud effects, and because of the continuous refresh of the polluted air which enters in contact with the cement surface. Hence, a key problem to solve in the application of photocatalysis in cementitious material for outdoor structures and buildings, is to increase the efficacy of the photocatalyst (particularly TiO_2-based) to tackle and partially compensate for its limited activity in real conditions. In this work, we overcame TiO_2 drawbacks, enhancing photocatalytic activity through the modification of TiO_2-NPs with graphene. Indeed, graphene is able to slow down the recombination of the photo-generated e/h pairs (Serpone et al., 1995), increasing the reactivity towards pollutants degradation. However, the big challenge of this work was to produce an efficient modification of TiO_2-NPs taking into consideration all the requirements for an industrial and scalable production of the enhanced photocatalyst. Indeed, the market in this sector is very sensitive to the high price and the large quantity of material needed. The insertion of a small quantity of graphene can, by enhancing the performance of the bare commercial titanium dioxide, increase or at least maintain the same performance of an already commercialized cement allowing to lower the TiO_2 content, thus the impact of the cost of the photocatalytic additive on cement. In order to meet price requirements, we decided to use graphite flakes (cost 1300 USD/Ton estimated for 2022, https://www.northerngraphite.com/about-graphite/graphite-pricing/) or partially exfoliated graphite as starting materials, using TiO_2-NPs as exfoliating agents to obtain graphene. With this method we found a convenient way to promote the interaction between TiO_2 and graphene and exfoliate graphite at the same time. The most promising techniques that matched the requirements of an effective production of graphene and an industrial scale up were ball milling (Leon et al., 2011, 2014; Quintana et al., 2013) and shear exfoliation (Paton et al., 2014; Yi and Shen, 2015). Different photocatalysts were produced with different ratios of TiO_2 /graphite starting material from 2% to 50% w/w of graphite with respect of the commercial TiO_2. We would like to stress that, because of the modest cost of graphite and the simplicity of the production process, the carbon-doped photocatalyst estimated price does not differ significantly from the bare TiO_2 one. A first screening of the TiO_2/graphite compositions was performed with NO_x degradation tests. Then, the most performing compounds were inserted into a concrete matrix. The characterization was performed on powders as well as on powders embedded in concrete. Morphological analysis was performed using scanning electron microscopy (SEM), while compositional analysis was based on the high-resolution powder X–ray diffraction (HR-PXRD) measured on powders. In order to assess the influence of the insertion of graphene on TiO_2 and compare the preparation methods, we tested the optical properties of the composites by UV/Vis absorbance. Finally, we monitored NO_x degradation to test the photocatalytic performances of the previously selected nanomaterials embedded in concrete matrixes,

Table 1
LAG powder compositions tested for NOx abatement, average photocatalytic abatement (Ac) and percentage of Ac increment compared to TiO_2 AHP 200 (LAG0).

Photocatalyst	TiO_2/G2Nan (w/w) dry matter	Average Ac	% of Ac increment compared to LAG0
LAG0	100	32	Reference
LAG2	50:1	42.3	32
LAG5	20:1	48.8	53
LAG10	10:1	55.6	74
LAG10-S‡,*	10:1	52.2*	80*

‡ "S" samples have a further step of sonication at the end of photocatalytic powder preparation.
* sample of a different batch- Ac % referred to the reference LAG0 (Average Ac= 29).

Table 2
MCG powder compositions tested for NOx abatement, average photocatalytic abatement (Ac) and percentage of Ac increment compared to TiO_2 AHP 200 (MCG00).

Photocatalyst	TiO_2/GF/Mel (w/w/w) dry matter	Average Ac	% of Ac increment compared to MCG00
MCG00	1:0:0	32	Reference
MCG11	1:0:1	38.1	19
MCG06	1:1:1	49.1	53
MCG06-S‡	1:1:1	47.2	48
MCG07	4:1:1	47.0	47
MCG16	1:2:1	44.3	38

‡ "S" samples have a further step of sonication at the end of photocatalytic powder preparation.

which gave a relevant increment in the photocatalytic activity compared to bare TiO_2. Scheme 1.

2. Results and discussion

2.1. NO_x powder test of LAG and MCG compounds with different doping level of graphene

Deposits of LAG and MCG powders, obtained respectively by shear exfoliation and ball milling, with different doping level of graphene, were tested for NO_x abatement in order to determine the effect of the composition on the photocatalytic activity. Results of the NO_x abatement for LAG and MCG powders are reported in Tables 1 and 2, respectively.

Tables 1 and 2 show the photocatalytic NO_x abatement (Ac) for each photocatalytic powder and compare the different samples relating their activity to the performance of the reference, corresponding to

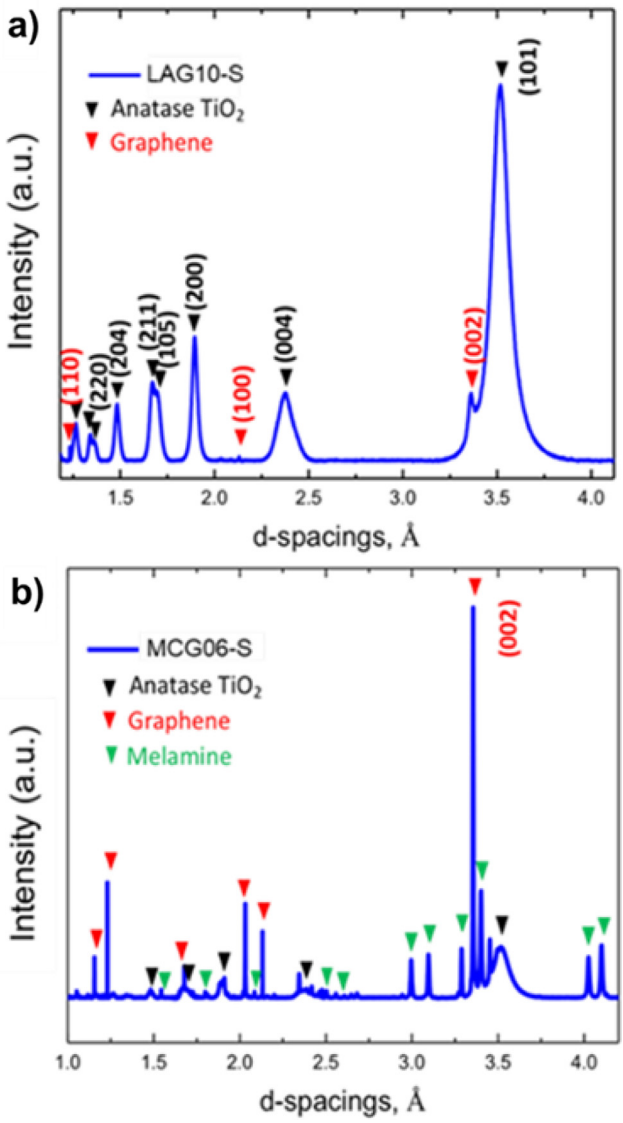

Fig. 1. HR-XRD patterns of LAG10-S (a) and MCG06-S (b). All the characteristic diffraction peaks of the identified phases are fully indexed.

commercial TiO_2 Hombikat 200 (AHP), named respectively LAG0 and MCG00 in Tables 1 and 2. Samples LAG10, LAG10-S and MCG06, MCG06-S showed the best photocatalytic activity, with an increase in Ac approx. 70% for LAG samples and 50% for MCG samples with respect to the bare TiO_2 activity. Therefore, these samples were selected among all the different TiO_2-graphene compositions tested. The sonication step, present in LAG10-S and MCG06-S, does not lead to remarkable differences in the photocatalytic activities compared to LAG10 and MCG06 powders but to a more uniform TiO_2/graphene distribution, which is relevant for the dispersion of the photocatalyst in the cementitious matrix. Thus, LAG10-S and MCG06-S, representing TiO_2-graphene best composites, have been further characterized and embedded in the cement matrix.

2.2. LAG10-S and MCG06-s powder characterization-HR-XRD

HR-XRD patterns were collected from LAG10-S and MCG06-S powders and are shown in Fig. 1.

In both LAG10-S and MCG06-S XRD patterns, typical anatase TiO_2 diffraction peaks (black) can be noticed, e.g. (101) facet, the prevalent one in anatase polymorph (JCPDS 21-1272). Typical graphite diffraction peaks (red) are also present in both samples (JCPDS 75-2078). MCG06-S also presents diffraction peaks corresponding to melamine (green), as expected.

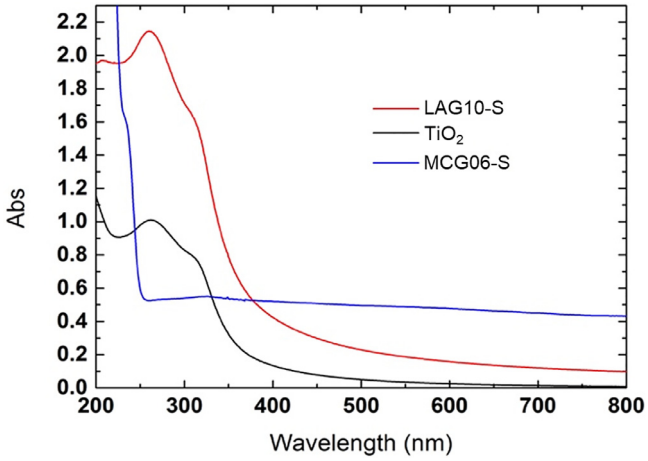

Fig. 2. UV-Vis spectra of TiO_2, LAG10-S and MCG06-S powder dispersions.

Table 3
Results for NOx abatement obtained for photocatalysts embedded in cement matrix (Italbianco 52.5R) (LAG10-SI and MCG06-SI samples).

Sample name	Photocatalyst (3% in cement)	% of Ac increment compared to AI
AI	TiO_2	Reference
LAG10-SI	LAG10-S	23±6%
MCG06-SI	MCG06-S	21±5%

2.2.1. UV-Vis characterization

UV-Vis characterization of LAG10-S and MCG06-S powder dispersions was performed (Fig. 2).

Fig. 2 shows the absorption profile of all the samples after 45 min of sonication in acidic environment and 10 min of centrifugation (2000 rpm). Comparing LAG10-S and TiO_2 spectra, a highly more intense band can be noticed in the former, denoting the presence of a higher quantity of TiO_2. This means that TiO_2, after the sonication and centrifugation process, has a better stability in LAG10-S than in bare TiO_2 aqueous dispersions. Regarding the MCG06-S sample, the collected spectrum refers to a dispersion obtained only by sonication, since, after centrifugation process, too little quantity of TiO_2 remained in solution to be easily detectable by an UV-Vis analysis. This denotes a low stability of MCG06-S powder in water: as expected, the reported spectrum displays an intense scattering phenomenon, implying the presence of more aggregated particles with respect to the other samples. The very intense band under 250 nm is referred to melamine (Li et al., 2015).

2.2.2. HR-SEM: photocatalysts in powder form

HR-SEM analysis was performed on LAG10-S and MCG06-S powders (Fig. 3). Both samples show the presence of TiO_2 deposited on graphene sheets, but LAG10-S shows a better distribution of TiO_2 on the top of graphene than MCG06-S.

This is in accordance with the higher stability of LAG10-S aqueous dispersion observed in UV-Vis characterization (Fig. 2) with respect to MCG06-S. Furthermore, it can explain the LAG10-S higher photocatalytic activity (Tables 3 and 4): the more uniform distribution of TiO_2 on the surface of graphene makes charge separation more effective due to better interaction of TiO_2 and graphene, while TiO_2 become more active because less aggregated. Therefore, it appears that graphene exfoliation is more successful when obtained by blender shear forces rather than by ball milling technique.

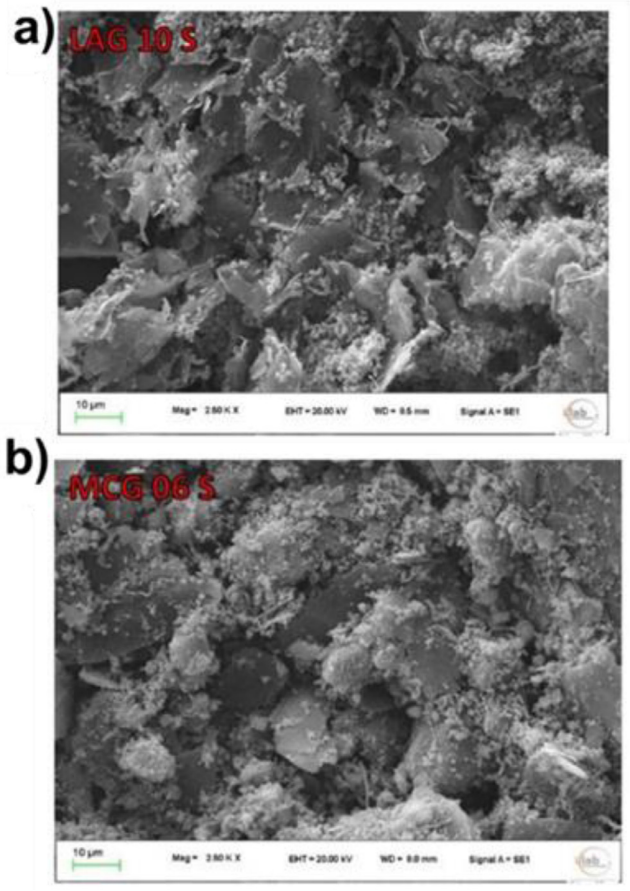

Fig. 3. SEM images of LAG10-S (a) and MCG06-S (b) powders.

Table 4
Results for NO_x abatement obtained for photocatalysts embedded in hydraulic lime matrix (LAG10-SC and MCG06-SC samples).

Sample name	Photocatalyst (3% in hydraulic lime)	% of Ac increment compared to AI
AI	TiO_2	Reference
LAG10-SC	LAG10-S	42±7%
MCG06-SC	MCG06-S	22±5%

2.3. Characterization of LAG10-s and MCG06-s embedded in lime and cement matrix

2.3.1. HR-SEM: Embedded photocatalysts

HR-SEM images of LAG10-S and MCG06-S embedded in cement matrix (Fig. 4) were collected to monitor the distribution of the photocatalyst on the cement surface. The acquisition was also performed in phase contrast mode using energy selective backscattered (EsB) detector (Fig. 4 – right panels). In images obtained by in-lens detector (left panels), graphene can be distinguished from the cement owing to its distinct morphology (red circles), while it is clearly detectable in images obtained by EsB detector (right panels) due to both the different morphology and its lower Z atomic number, which generates a clear contrast (dark area - yellow dotted circles). Therefore, this analysis reveals the presence of graphene on the cement surface of both LAG10-S and MCG06-S. LAG10-S was also embedded in lime matrix and its distribution was also observed by HR-SEM (Fig. 4), clearly showing its presence.

2.3.2. Micro – Raman

Micro–Raman analysis, performed on the LAG10-S and MCG06-S in cement (Fig. 5) and lime matrices, also confirmed the presence of the photocatalyst on the surface.Indeed, typical Raman peaks of Titania (Naldoni et al., 2012) and graphene (Ferrari et al., 2006) are observed in both spectra in Fig. 5 and melamine peaks (Schneider and Schrader, 1975) are also present in MCG06-S sample (Fig. 5a).

2.3.3. Energy dispersive X-ray spectroscopy (EDS)

EDS quantitative analysis on TiO_2 (AHP200), LAG10-S and MCG06-S samples embedded in cementitious matrix was performed. This analytical technique is used for elemental analysis or chemical mapping of a surface, to quantify the elements of interest. TiO_2, LAG10-S and MCG06-S were embedded in cementitious samples with a thickness of 13 mm. EDS mapping was performed on each side of the samples, to study the distribution of the photocatalyst through the cement matrix (Fig. 6). Results showed an unexpected distribution of the photocatalysts on the upper and the lower surfaces of the cementitious matrix. Indeed, while 3.8% of TiO_2 on the top of the reference sample was observed, in LAG10-S and MCG06-S TiO_2 the quantity detected by EDS (Cameo+ function) are 0.8% and 0.1%, respectively. These outcomes might be due to a different migration of the photocatalyst powder across the matrix during the hardening phase of the cement. In order to minimize the effect of the anisotropic distribution of the photocatalyst into the matrix, cementitious samples with a thickness of 1 mm were used for the NO_x abatement test.

2.4. NO_x abatement test of LAG10-s and MCG06-s embedded in lime and cement matrix

Photodegradation of inorganic pollutants (NO_x) was tested on LAG10-S and MCG06-S incorporated in cement or hydraulic lime. TiO_2 (AHP200) was also tested as a reference. Results of NO_x for cement matrix and hydraulic lime are reported respectively in Tables 3 and 4.

As observed in Tables 3 and 4, LAG10-S and MCG06-S show an increase in the photocatalytic activity of at least 20% with respect to that of TiO_2, when embedded in cement as well in hydraulic lime. Furthermore, it is worth noting that LAG10-S, which is the most performing photocatalyst, displays a 42% increase of photocatalytic activity in hydraulic lime matrix with respect to TiO_2.

3. Experimental section

3.1. Photocatalysts preparation

Two families of TiO_2-graphene photocatalysts called MCG and LAG, were produced respectively by ball milling and shear exfoliation. MCG photocatalysts were prepared with a Pulverisette 6 ball mill apparatus, and Titanium dioxide (AHP200 from Sachtleben Chemie), Gaphite flakes (GF) from Sigma Aldrich with an average dimension of +100 mesh and Melamine (Mel) from Alfa Aesar with a purity of >99%. Melamine is introduced in the ball mill to promote graphite exfoliation (Leon et al., 2011, 2014). A composition (15 g) of the ingredients was introduced in a Zircomiun jar (250 ml) containing Zirconium balls ranging from 5 to 20 mm (n°10 of φ5mm+n°15 of φ10mm+n°6 of φ20mm). The composition was then milled in a planetary mill for1 cycle at 150 rpm for 45 min (Leon et al., 2011). Only for MCG06-S, the photocatalyst (7 g) was subsequently mixed with 2-propanol (100 ml) for 10 min and the dispersion was thereafter sonicated for 4 h and was then dried at 60 °C. The product was milled in a centrifugal mill at 150 rpm for 45 min. MCG00 and MCG11 were produced as references. The photocatalysts of the series LAG were prepared adding G2Nan paste purchased by Nanesa (4% dry graphene like matter) and TiO_2 powder (AHP200 from Sachtleben Chemie with average surface area of 160–240 m^2/g and anatase purity>90%) to water, to produce an aqueous slurry. The slurry was then mixed in a laboratory blender at 11,000 rpm for 40 min and was dried at 60 °C. In the LAG10-S sample the obtained powder was next sonicated for 4 h in 2-propanol and subsequently dried at 60 °C.

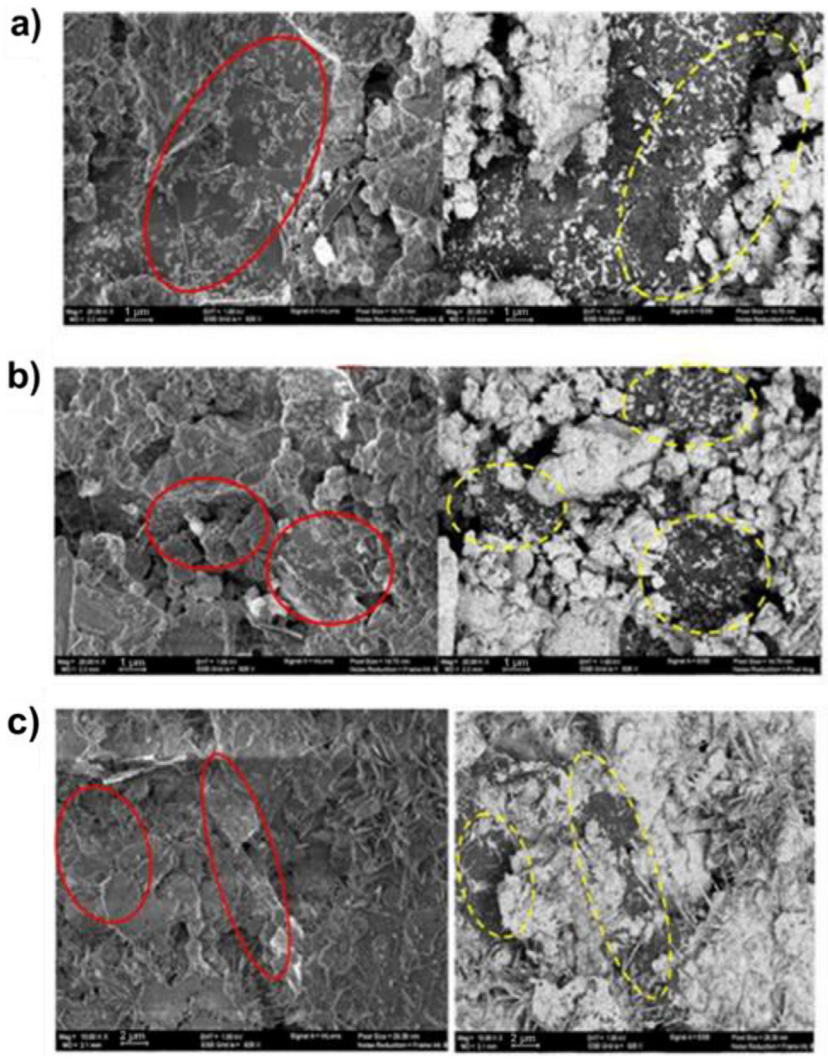

Fig. 4. Images obtained by in-lens (left panels) and energy selective backscattered detector (EsB; right panels). (a) LAG10-S sample in cement matrix. (b) MCG06-S sample in cement matrix. (c) LAG10-S sample in hydrated lime. Red circles and yellow dotted circles highlight respectively difference in graphene and cement matrix in morphology (in-lens) and in contrast (EsB).

3.2. Mortar sample preparation

The fresh cementitious mixture was mortar prepared according to the procedure described in the standard UNI EN 196–1, replacing part of the cement with the photocatalyst. All the photocatalytic compounds were incorporated in a binder matrix: white cement i.design Italbianco 52.5R ("I" samples, e.g. LAG10I) or hydraulic lime matrix i.pro chaux pure NHL5 ("C" samples). The following composition were used: 1 part of hydraulic cement or lime binder, 3 parts of sand, 0.5 parts of water, 0.36% w/w (with respect of the binder) of cellulose and 3.0% w/w of TiO_2 (with respect of the binder). The fresh mortar was poured into the lid of a Petri capsule and maintained in a conditioned room at 20 °C and 90% relative humidity (RH) for 7 days. Then the sample was left at 20 °C and 60% of RH for all the time before the measurement.

3.3. UV-Vis spectroscopy

UV-Vis absorption spectra of aqueous dispersion of TiO_2 MCG06-S and LAG10-S were recorded by means of a Perkin Elmer Lambda 40 UV-Vis spectrophotometer. The samples were prepared by sonicating 2 mg/mL dispersions of the photocatalysts in acidic water (HCl 0.01 M) for 45 min. Then samples were centrifuged for 10 min (2000 rpm); the supernatant solution (almost 1 mg/mL) was then diluted to 0.2 mg/mL to collect the spectra. MCG06-S powder in water was just sonicated and diluted to collect the spectrum.

3.4. NO_x abatement method

The photocatalytic activity of TiO_2 photocatalyst in powders and incorporated cement-based materials was evaluated by NO_x abatement adopting the continuous flow procedure using the apparatus reported in the Italian standard UNI 11,247, and schematized in Fig. 7, (Bellardita et al., 2010) that describes a method aimed at assessing the index of photocatalytic abatement due to the action of inorganic materials. As far as the NO_x abatement is concerned, the experimental set up is reported in Fig. 7. The scheme illustrates a batch recirculation system where a certain concentration of NO_x was first introduced with air in a large volume chamber (C, 20 L) and after mixing (recirculation via routes 1–2), the test gaseous mixture was allowed to circulate (4.5 Lmin−1) through the reaction chamber (R) (routes 1–3) in the dark, and analyzed at established time intervals (routes 1–4). For the photocatalytic tests, the catalyst sample was positioned in the reaction chamber R which was provided with an optical window for illumination. The NO_x concentration was detected by a chemiluminescence analytical method by a Nitrogen Oxides Analyzer Environment SA AC32M instrument. (Bellardita et al., 2010) The sample to be investigated was collocated inside a reaction chamber containing an irradiation system that provides an average irradiance (in UV-A band) of (20±1) W/m^2 on the specimen surface (64cm^2) during the test. The irradiation source is a Mercury lamp Radium Sanolux HRC 300–280 E27 UV-lamp, with an irradiance (I) both in UVA (280nm- 315 nm; I = 3 W/m^2 at 0.5 m) and UVB

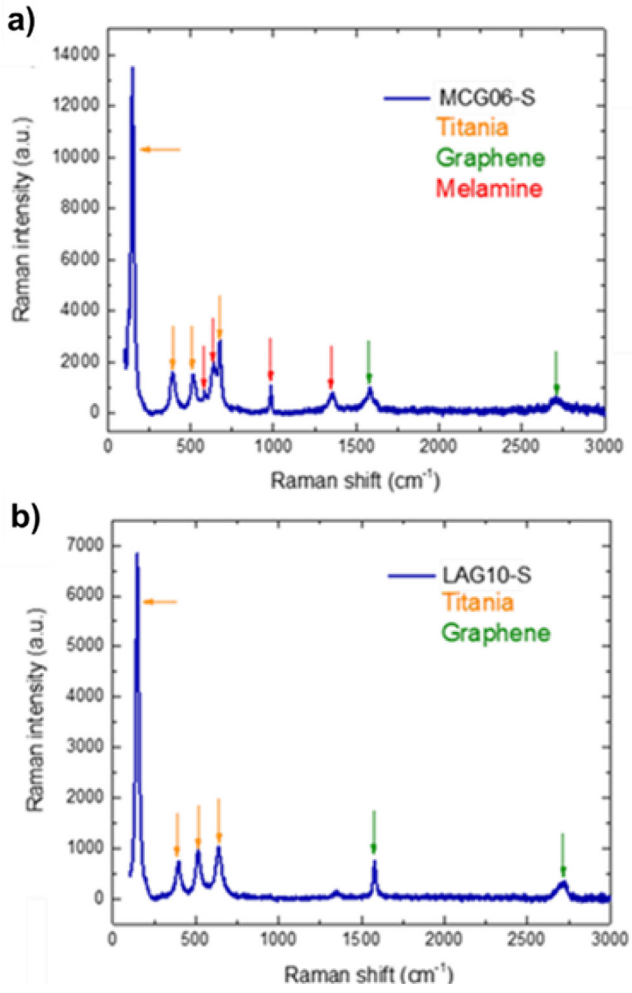

Fig. 5. Raman spectrum of graphene edge, carried on cement matrix for MCG06-S (a) and LAG10-S (b).

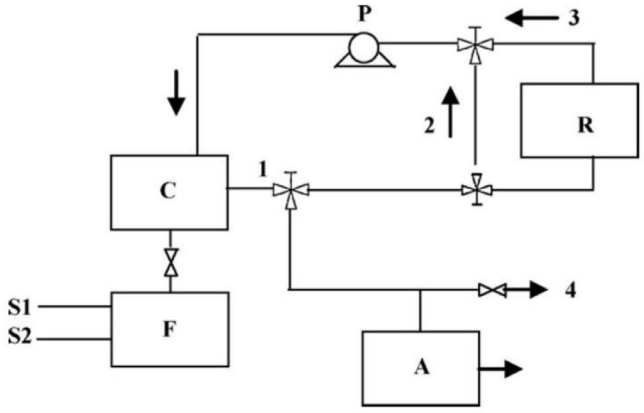

Fig. 7. Experimental setup for NO_x measurements. In this scheme, letters indicate: NO_x ($NO+NO_2$); source (S1); pure air (S2); flux meter (F); gas mixing chamber (C); reaction chamber (R); NOx analyzer (A); membrane pump (P).

(315–400 nm; $I = 13.6$ W/m^2 at 0.5 m). In the UV (λ<400 nm) irradiance spectrum the main component is the 365 nm line signal brought by the presence of mercury inside of the lamp (according to the standard UNI 11,247 irradiance integrated at λ <350 nm is forecast to be 10% lower than the irradiance integrated between 350 and 400 nm). In the standardized continuous flow procedure according to UNI 11,247, the flow of polluted air containing 0.55 ppm of NO_x (of which NO_2=0.15 ppm and NO=0.4 ppm) was constant (1.5 litre/min). The first phase of the test was performed in dark conditions to equalize the adsorption processes and to achieve a constant gas flow and NO_x concentration (CB). During this first phase in dark conditions, the concentration of the gas entering and leaving the reactor was constantly measured. When the concentration of the outlet gas from the reactor was stable, the second phase of the test started and the lamp was switched on. At this stage, the system could balance for a certain time to reach an equilibrium gas concentration (CL). The difference between the NO_x concentration measured in the dark and the light phase allowed to calculate the A_C index of the photocatalytic abatement since the illumination activated the photocatalytic reactions, which led to the degradation of the NO_x. The

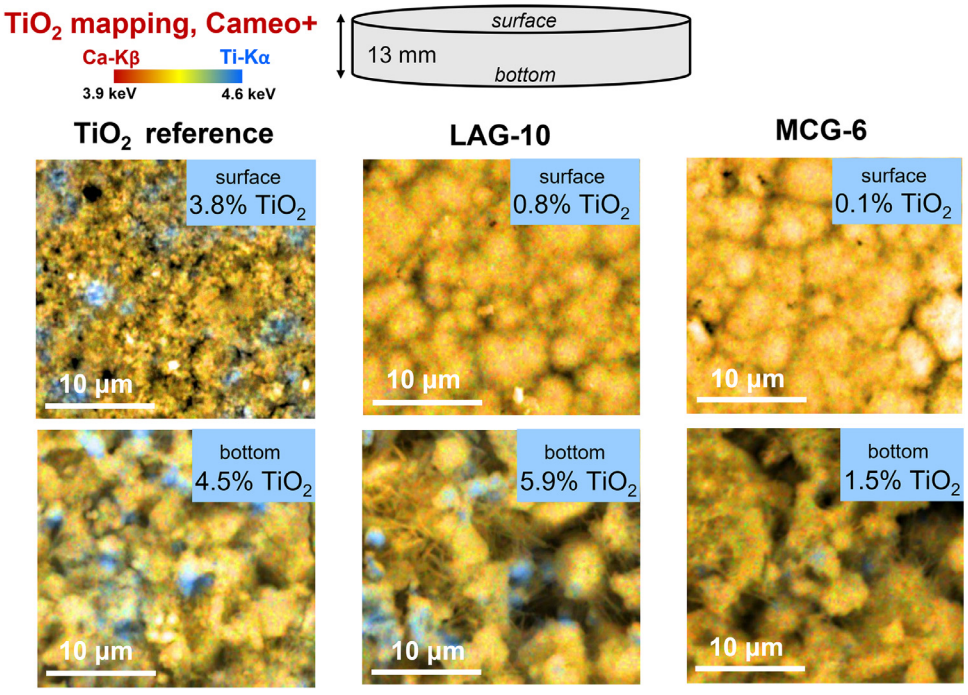

Fig. 6. Portions of surface and bottom of cementitious samples with TiO_2 (AHP200), LAG10-S and MCG06-S mapped with EDS.

photocatalytic abatement A_C is (Eq. (1)):

$$A_C = 100 * \frac{(C_B - C_L)}{C_B} * \frac{Ir_N}{Ir} * \frac{SA_N}{SA} \quad (1)$$

Where A_C is the photocatalytic abatement index under test conditions (%), C_B is the constant NO_x concentration at the reactor exit in dark conditions (ppb), C_L is the constant NO_x concentration at the reactor exit under radiation (ppb), Ir is the average irradiance as measured and corrected (W m^{-2}), Ir_N is the nominal irradiance (20 W m^{-2}), SA is surface area of the specimen as measured (cm^2) and SA_N is the nominal surface area of the specimen (61 cm^2). In the case of tests on photocatalyst in powder, the preparation occurred by 10 min bath sonication with BANDELIN SONOREX (frequency of 35 kHz and power 80/320 W) of a mixture of 1.5 g of powder with 2-propanol (20 ml). Then the very slow drying process of the mixture deposited on the bottom of a Petri glass, approx. φ=8.8 mm (area =61 mm^2), allowed the formation of a homogeneous and continuous deposit, ready for the measurement of Ac.

3.5. High resolution powder X-ray diffraction (HR-PXRD)

X-ray diffraction experiments were conducted at the ID22 beamline of the European Synchrotron Research Facility (ESRF), Grenoble, France. The experiments were carried out at a wavelength of 0.39999 (168) Å. Cementitious samples were powdered and loaded into borosilicate capillaries of 1 mm in diameter, and their X-ray diffraction patterns were collected.

3.6. High resolution scanning electron microscopy (HR-SEM)

For the HR-SEM analysis, we used a Zeiss Ultra-Plus FEG-SEM. HR-SEM analysis enabled imaging of graphene areas on the surface of the samples employing the energy selective backscattered (EsB) detector. The latter allowed observation of the compositional contrast between graphene and cement matrix.

3.7. Energy-dispersive X-ray spectroscopy (EDS)

FFEI E-SEM Quanta 200 an environmental SEM equipped with EDS detector was used for elemental mapping performed at the x5000 magnification, accelerating voltage of 20 kV and spot size 6. Elemental mapping of the upper and bottom surfaces of the cementitious samples were obtained utilizing mapping utility of the INCA software built in the Quanta microscope. Specifically, we used Cameo+ utility, which allows user to see the chemical composition and topography in one image. The fine detail of the electron image is shown together with a full color overlay showing variation in the X-ray spectrum, which can indicate compositional changes. Individual X-ray photons are assigned a color, which depends on their energy. A color range for Cameo+ is selected by entering a value for the lowest energy which defines where the red part of the color scale starts, and the higher energy which defines the end of the blue part of the scale. As an example, in the case of a Cameo map of TiO_2 distribution starting red part (lowest energy) was assigned to Ca-K_β and end of the blue part corresponded to Ti-K_α (highest energy). Ca-Ti Cameo+ element maps were obtained in the energy range of 3.9–4.6 keV.

3.8. Micro-Raman measurements

We used a HORIBA Jobin Yvon (LabRAM HR Evolution®) Micro-Raman, equipped with a 532 nm laser and a 50x microscope objective. A silicon wafer was used to calibrate the instrument. The spectra were acquired with a grating of 1800 gr mm^{-1}, at an acquisition rate of 200 s, and averaged from three spectra accumulations.

4. Conclusions

In this work, we successfully developed novel photocatalytic nanomaterials for application in self-cleaning cements by industrially scalable methods. TiO_2-modified cementitious materials are already present in the market:considered that the cost of cement is about 130 USD/Ton, in the case of 3% TiO_2 doping the cost of the photocatalyst is about 100 USD/Ton, which is already accepted by the market. The cost of the carbon-doped photocatalysts we present here can be estimated to be similar o even lower than this, offering, as an advantage, a higher photoactivity. The nanocomposites we developed, may replace bare TiO_2 as building materials for the photodegradation of pollutants and in particular of NO_x, mainly produced by combustions engines of the cars, in the city of the future. These materials may also offer performances equal to TiO_2 at lower dosage. To summarize, we improved TiO_2 photocatalytic efficiency by modifying it with graphene, already well known for its beneficial interaction with titania. We were able to obtain an excellent graphene exfoliation and interaction with TiO_2 by means of easy, low-cost and scalable procedures of ball milling and shear mixing. The activity of various graphene/TiO_2 compositions obtained with the two exfoliation methods have been investigated towards NO_x abatements. The two most performing powders, LAG10-S, obtained by shear mixing, and MCG06-S, obtained by ball milling, were further characterized and embedded in cement and hydraulic lime. HR-SEM and Raman measurements confirmed that both photocatalysts are uniformly distributed on the cementitious surface; EDS showed less uniformity of the distribution through the thickness of the cementitious sample, problem that could be overcome by additives, such as cellulose, to avoid settling effect. Photocatalytic tests of cement and hydraulic lime modified by LAG10-S and MCG06-S towards NO_x abatement resulted in an enhancement of at least 20% with respect of TiO_2 embedded in the same matrices. In summary, we report on the approach to obtain novel TiO_2-graphene photocatalysts that confer a significant improvement in the photocatalytic performance of cementitious matrixes for outdoor air remediation. The photocatalysts can be obtained by easily scalable methods, which considerably reduces the production cost and thus increases their applicability in industry.

Environmental implication statement

Elimination of air pollutants is a hot topic of environmental chemistry and, at research level, TiO_2 modification by graphene has been widely studied to improve photocatalytic activity. However, application of these systems is still lacking. Herein, TiO_2-graphene nanocomposites have been embedded in a cement matrix as photocatalytic coatings for air remediation. They were synthesized exfoliating graphite and optimizing graphene-TiO_2 adhesion in a single step, low-cost and scalable process. These new TiO_2-graphene nanocomposites show a significative improvement in the photocatalytic degradation of air contaminants with respect to bare TiO_2, even when embedded in complex matrixes like cements.

Declaration of Competing Interest

The authors declare the following financial interests/personal relationships which may be considered as potential competing interests

European Patent EP3216771A1.

Funding

This work was supported by the European Union Seventh Framework Program Graphene Flagship Core 1 and Core 2 [grant number 604391]

References

Bellardita, M., Addamo, M., Di Paola, A., Marcì, G., Palmisano, L., Cassar, L., Borsa, M., 2010. Photocatalytic activity of TiO_2/SiO_2 systems. J. Hazard. Mater. 174, 707–713.

Chen, M., Chu, J.W., 2011. NOx photocatalytic degradation on active concrete road surface - from experiment to real-scale application. J. Clean. Prod. 19 (11), 1266–1272. doi:10.1016/j.jclepro.2011.03.001.

Chen, X., Mao, S.S., 2007. Titanium dioxide nanomaterials: synthesis, properties, modifications, and applications. Chem. Rev. 107 (7), 2891–2959. doi:10.1021/cr0500535.

Dalton, J.S., Janes, P.A., Jones, N.G., Nicholson, J.A., Hallam, K.R., Allen, G.C., 2002. Photocatalytic oxidation of NOx gases using TiO_2: a surface spectroscopic approach. Environ. Pollut. 120 (2), 415–422. doi:10.1016/s0269-7491(02)00107-0.

Dylla, H., Hassan, M.M., Schmitt, M., Rupnow, T., Mohammad, L.N., 2011. Laboratory investigation of the effect of mixed nitrogen dioxide and nitrogen oxide gases on titanium dioxide photocatalytic efficiency in concrete pavements. J. Mater. Civ. Eng. 23 (7), 1087–1093. doi:10.1061/(asce)mt.1943-5533.0000248.

Ferrari, A.C., Meyer, J.C., Scardaci, V., Casiraghi, C., Lazzeri, M., Mauri, F., Piscanec, S., Jiang, D., Novoselov, K.S., Roth, S., Geim, A.K., 2006. Raman spectrum of graphene and graphene layers. Phys. Rev. Lett. 97 (18). doi:10.1103/physrevlett.97.187401.

Fleisch, M., Bahnemann, D., 2017. Photocatalitically active concrete: how innovative construction materials can contribute to the degradation of dangerous air pollutants. Beton Stahlbetonbau 112, 47–53. doi:10.1002/best.201600506.

Folli, A., Jakobsen, U.H., Guerrini, G.L., Macphee, D.E., 2009. Rhodamine B discolouration on TiO_2 in the cement environment: a look at fundamental aspects of the self-cleaning effect in concretes. J. Adv. Oxid. Technol. 12 (1), 126–133. doi:10.1515/jaots-2009-0116.

Folli, A., Pade, C., Hansen, T.B., De Marco, T., Macphee, D.E., 2012. TiO_2 photocatalysis in cementitious systems: insights into self-cleaning and depollution chemistry. Cem. Concr. Res. 42 (3), 539–548. doi:10.1016/j.cemconres.2011.12.001.

Fujishima, A., Zhang, X.T., Tryk, D.A., 2008. TiO_2 photocatalysis and related surface phenomena. Surf. Sci. Rep. 63 (12), 515–582. doi:10.1016/j.surfrep.2008.10.001.

Hoffmann, M.R., Martin, S.T., Choi, W.Y., Bahnemann, D.W., 1995. Environmental applications of semiconductor photocatalysis. Chem. Rev. 95 (1), 69–96. doi:10.1021/cr00033a004.

Husken, G., Hunger, M., Brouwers, H.J.H., 2009. Experimental study of photocatalytic concrete products for air purification. Build. Environ. 44 (12), 2463–2474. doi:10.1016/j.buildenv.2009.04.010.

Kovar, P., Lacny, Z., Prikryl, J., Matejka, V., 2010. The Route for the decreasing of air pollutants using photocatalysis over titanium dioxide incorporated into different kinds of concrete surfaces. Iv Czech Slovak Sci. Conf. Transp. Health Environ. 1, 133–138.

Lai, Y.K., Huang, J.Y., Cui, Z.Q., Ge, M.Z., Zhang, K.Q., Chen, Z., Chi, L.F., 2016. Recent advances in TiO_2-based nanostructured surfaces with controllable wettability and adhesion. Small 12 (16), 2203–2224. doi:10.1002/smll.201501837.

Leon, V., Quintana, M., Herrero, M.A., Fierro, J.L.G., de la Hoz, A., Prato, M., Vazquez, E., 2011. Few-layer graphenes from ball-milling of graphite with melamine. Chem. Commun. 47 (39), 10936–10938. doi:10.1039/c1cc14595a.

Leon, V., Rodriguez, A.M., Prieto, P., Prato, M., Vazquez, E., 2014. Exfoliation of graphite with triazine derivatives under ball-milling conditions: preparation of few-layer graphene via selective noncovalent interactions. ACS Nano 8 (1), 563–571. doi:10.1021/nn405148t.

Li, Y., Cheng, L., Liu, C., Liu, W., Zhu, L., Fan, Y., Wu, Y., Li, X., Zeng, Q., Fan, X., 2015. Supramolecular three-component amino acid-based hydrogels with superior mechanical strength for controllably promoting nonpathogenic E. coli growth. RSC Adv. 5 (118), 97629–97634. doi:10.1039/c5ra13827b.

Linsebigler, A.L., Lu, G.Q., Yates, J.T., 1995. Photocatalysis on TiO_2 surfaces - principles, mechanisms, and selected results. Chem. Rev. 95 (3), 735–758. doi:10.1021/cr00035a013.

Mamaghani, A.H., Haghighat, F., Lee, C.S., 2017. Photocatalytic oxidation technology for indoor environment air purification: the state-of-the-art. Appl. Catal. B Environ. 203, 247–269. doi:10.1016/j.apcatb.2016.10.037.

Naldoni, A., Allieta, M., Santangelo, S., Marelli, M., Fabbri, F., Cappelli, S., Bianchi, C.L., Psaro, R., Dal Santo, V., 2012. Effect of nature and location of defects on bandgap narrowing in black TiO_2 nanoparticles. J. Am. Chem. Soc. 134 (18), 7600–7603. doi:10.1021/ja3012676.

Paton, K.R., Varrla, E., Backes, C., Smith, R.J., Khan, U., O'Neill, A., Boland, C., Lotya, M., Istrate, O.M., King, P., Higgins, T., Barwich, S., May, P., Puczkarski, P., Ahmed, I., Moebius, M., Pettersson, H., Long, E., Coelho, J., O'Brien, S.E., McGuire, E.K., Sanchez, B.M., Duesberg, G.S., McEvoy, N., Pennycook, T.J., Downing, C., Crossley, A., Nicolosi, V., Coleman, J.N., 2014. Scalable production of large quantities of defect-free few-layer graphene by shear exfoliation in liquids. Nat. Mater. 13 (6), 624–630. doi:10.1038/nmat3944.

Poon, C.S., Cheung, E., 2007. NO removal efficiency of photocatalytic paving blocks prepared with recycled materials. Constr. Build. Mater. 21 (8), 1746–1753. doi:10.1016/j.conbuildmat.2006.05.018.

Quintana, M., Vazquez, E., Prato, M., 2013. Organic functionalization of graphene in dispersions. Acc. Chem. Res. 46 (1), 138–148. doi:10.1021/ar300138e.

Ramirez, A.M., Demeestere, K., De Belie, N., Mantyla, T., Levanen, E., 2010. Titanium dioxide coated cementitious materials for air purifying purposes: preparation, characterization and toluene removal potential. Build. Environ. 45 (4), 832–838. doi:10.1016/j.buildenv.2009.09.003.

Schneider, J.R., Schrader, B., 1975. Measurement and calculation of the infrared and raman active molecular and latice vibrations of the crystalline melamine(1,3,5-triamino-s-triazine). J. Mol. Struct. 29 (1), 1–14. doi:10.1016/0022-2860(75)88001-X.

Serpone, N., Lawless, D., Khairutdinov, R., 1995. Size effects on the photophysical properties of colloidal anatase TiO_2 particles - size quantization or direct transitions in this indirect semiconductor. J. Phys. Chem. 99 (45), 16646–16654. doi:10.1021/j100045a026.

Tong, H., Ouyang, S.X., Bi, Y.P., Umezawa, N., Oshikiri, M., Ye, J.H., 2012. Nano-photocatalytic materials: possibilities and challenges. Adv. Mater. 24 (2), 229–251. doi:10.1002/adma.201102752.

Tuchinda, C., Srivannaboon, S., Lim, H.W., 2006. Photoprotection by window glass, automobile glass, and sunglasses. J. Am. Acad. Dermatol. 54 (5), 845–854. doi:10.1016/j.jaad.2005.11.1082.

Yi, M., Shen, Z.G., 2015. A review on mechanical exfoliation for the scalable production of graphene. J. Mater. Chem. A 3 (22), 11700–11715. doi:10.1039/c5ta00252d.

Yu, C.L., Zhou, W.Q., Liu, H., Liu, Y., Dionysiou, D.D., 2016. Design and fabrication of microsphere photocatalysts for environmental purification and energy conversion. Chem. Eng. J. 287, 117–129. doi:10.1016/j.cej.2015.10.112.

Zailan, S.N., Mahmed, N., Abdullah, M.M.A., Sandu, A.V., Shahedan, N.F., 2016. Review on characterization and mechanical performance of self-cleaning concrete. Eng. Technol. Int. Conf. (ETIC).

Zouzelka, R., Chemagazin, s.r.o., 2016. The photocatalytic abatement of NOx imissions using commercial functional coating with porous morphology. In: Proceedings of the ix. Konference Pigmenty a Pojiva, pp. 19–21.